

Article

Energy Bus-Based Matrix Modeling and Optimal Scheduling for Integrated Energy Systems

Lizhi Zhang  and Fan Li * 

School of Control Science and Engineering, Shandong University, Jinan 250061, China; 201920499@mail.sdu.edu.cn

* Correspondence: lifan1212@sdu.edu.cn

Abstract: Integrated energy systems (IESs) can easily accommodate renewable energy resources (RESs) and improve the utilization efficiency of fossil energy by integrating various energy production, conversion, and storage technologies. However, the coupled multi-energy flows and the uncertainty of RESs bring challenges regarding optimal scheduling. Therefore, this study proposes an energy bus-based matrix-modeling method and a coordinated scheduling strategy for the IES. The matrix-modeling method can be used to formulate the steady- and transient-state balances of the multi-energy flows, and the transient model can clearly express the multi-time-scale characteristics of the different energy flows. The model parameters are fitted with data from experiments and the literature. To address the inherent randomness of the RESs and loads, a coordinated scheduling strategy is designed that contains two components: day-ahead optimization and rolling optimization. Day-ahead optimization uses the system steady-state model and multiple scenarios from the RES and load forecast data to minimize the operation cost while rolling optimization is based on the system's transient-state model and aims to achieve the optimal real-time scheduling of the energy flows. Finally, a case study is conducted to verify the advantages and effectiveness of the proposed model and optimization method. The results show that stochastic optimization reduces the total daily cost by 1.48% compared to deterministic optimization when considering the prediction errors associated with the RESs and loads, highlighting the stronger adaptability of stochastic optimization to prediction errors. Moreover, rolling optimization based on the system's transient-state model can reduce the errors between day-ahead scheduling and rolling correction.

Keywords: integrated energy system; matrix model; optimal scheduling; day-ahead optimization; rolling optimization



Citation: Zhang, L.; Li, F. Energy Bus-Based Matrix Modeling and Optimal Scheduling for Integrated Energy Systems. *Appl. Sci.* **2024**, *14*, 4297. <https://doi.org/10.3390/app14104297>

Academic Editor: Andreas Sumper

Received: 27 April 2024

Revised: 12 May 2024

Accepted: 16 May 2024

Published: 19 May 2024



Copyright: © 2024 by the authors. Licensee MDPI, Basel, Switzerland. This article is an open access article distributed under the terms and conditions of the Creative Commons Attribution (CC BY) license (<https://creativecommons.org/licenses/by/4.0/>).

1. Introduction

An integrated energy system (IES) is an efficient tool to accommodate more renewable energy and improve the utilization efficiency of fossil energy [1]. It has received great attention in recent years, especially regarding its use in combination with high proportions of photovoltaic (PV) and wind power (WP) [2]. By integrating multiple types of energy conversion devices, the IES can flexibly convert natural gas, electricity, and heat energy and supply diverse types of energy for users simultaneously [3]. However, the complementary operation of these devices requires an intelligent energy management system or an optimal scheduling strategy.

Optimal scheduling requires an effective model that can clearly describe the complex structure of the IES and the coupled energy flows. In 2007, Geidl et al. [4] put forward the concept of an energy hub (EH), which describes the energy input, output, storage, and coupling relationships in the IES. Wang et al. [5] proposed a standardized matrix-modeling method for the IES, based on the concept of the EH, that is suitable for computer implementation and can facilitate the optimal scheduling of complex IESs. Liu et al. [6] presented an efficient standardized multi-step modeling method for the EH and separated a complex

EH model into several simple models based on the node arrangement and virtual node insertion methods, seeking to avoid large matrix calculations. Wang et al. [7] developed an automatic and linearized modeling method to formulate the energy conversion in the EH, and they quantitatively evaluated the flexibility of the system based on the ranks of the coupling matrices. Ma et al. [8] improved the linearization model of the EH, expounding and simplifying the identification and selection of state variables. Li et al. [9] built an improved layering energy hub model for an electricity–heat–cold–gas coupled IES, which had the advantage of linear convexity compared to classical EH models, improving the solving efficiency.

The EH is also a promising option for the energy management of IESs [10,11]. The optimal scheduling strategies of residential and industrial EHs were developed to minimize the total energy consumption or demand charges [12,13]. Vahid-Pakdel et al. [14] established a stochastic optimization model for the EH operation and employed the CPLEX solver of the GAMS software to find the global optimum solution. Rastegar et al. [15] proposed a new framework for home energy management in the context of the residential EH using a probabilistic optimization approach. Brahman et al. [16] developed a thermal and electrical energy management strategy to optimally schedule major components of the EH. Ma et al. [17] proposed a novel matrix-modeling method based on graph theory to formulate the steady-state balance of energy flows in the IES, and they presented an optimal scheduling model in matrix form to minimize the daily operation cost. Luo et al. [18] presented a hierarchical Stackelberg game method to formulate the energy scheduling optimization of a three-level IES based on the EH model. Dini et al. [19] proposed an optimization model for the flexible and reliable operation of an electricity–gas–heat coupled EH with renewable energy sources. Salehemaleh et al. [20] developed a shrinking-horizon optimization framework for EH scheduling and used the DICOPT solver to determine the optimal scheduling scheme, which significantly improved the economic performance of the system. However, these studies based on EH models separately analyze and model the balances of the electricity, cooling, and heating flows in IESs, and the modeling processes and results are somewhat complex.

From the perspective of IESs, a combined cooling, heating, and power (CCHP) system is a typical component that supplies multiple types of energy by using various energy conversion technologies [21]. Chicco et al. [22] presented a comprehensive input–output matrix approach to model a small-scale trigeneration system, considering the interactions among the plant components and energy networks. Liu et al. [23] used conversion matrices, including the dispatch factors and component efficiencies, to describe the energy conversion and transfer processes of the CCHP system. Meng et al. [24] proposed a day-ahead scheduling optimization method for a park-level electricity–heat coupled IES, considering a flexible supply. Bao et al. [25] established day-ahead scheduling and real-time scheduling models for the CCHP microgrid and adopted scheduling schemes with different time scales in the real-time scheduling of cooling and electricity, seeking to address the fluctuations in renewable energy resources (RESs) and user loads. Luo et al. [26] proposed a novel two-stage coordinated control approach for CCHP energy management, including an economic dispatching stage (EDS) and a real-time adjusting stage (RTAS), in which the RTAS is used to adjust the scheme of the EDS to tackle power fluctuations. Gu et al. [27] proposed an online optimal scheduling approach based on model predictive control for CCHP microgrids, which can compensate for prediction errors in the RESs and loads. Li et al. [28] developed a hybrid time-scale energy management approach for IESs, which was composed of a day-ahead robust optimal scheduling model and an intraday rolling model. Hu et al. [29] presented the multi-time-scale optimization of IESs based on distributed model predictive control, which improved the economic performance of the system's operation. Song et al. [30] proposed a multi-time-scale scheduling approach for IESs considering the uncertainty of the RESs and loads, achieving low-carbon and economical supply–demand matching. Li et al. [31] presented a multi-time-scale optimization dispatch model for an IES, considering a demand response mechanism. Wang et al. [32]

constructed a multi-time-scale optimization model with day-ahead, intraday, and real-time scheduling based on a dynamic EH model, improving the accuracy of the system's operation significantly.

In the abovementioned research works, the models of the IES or EH are formulated based on steady-state balances of the energy flows, and the optimal scheduling problems include a day-ahead scheduling stage and a real-time scheduling stage. Due to the fluctuations in the RESs and loads, stochastic optimization methods are used in the day-ahead scheduling stage, while real-time scheduling mainly focuses on how to follow the variations. However, the different energy flows have different time-scale characteristics. For example, the electricity flow can reach a steady state in several seconds, but the heat flow needs several minutes or even an hour. In [25], the real-time scheduling method uses different cycle times to address the multi-time-scale characteristics. In other methods, the multi-time-scale characteristics are somewhat disregarded, leading to an inability to characterize the dynamic differences between electricity, heat, and gas. These methods are not able to achieve optimal real-time scheduling for the cooling or heat flow.

To resolve this issue, this paper proposes an energy bus-based matrix-modeling method and a coordinated scheduling strategy for the IES. The steady- and transient-state balances of the energy flows are formulated using the matrix-modeling method, whose parameters are fitted with data from experiments and the literature. To address the fluctuations in the RESs and loads, the coordinated scheduling strategy consists of two components: day-ahead optimization and rolling optimization. Day-ahead optimization uses the steady-state model and multiple scenarios concerning the RES and load forecast data. Rolling optimization is based on the transient-state model, aiming to achieve the optimal real-time scheduling of the energy flows, because the transient model can clearly reflect the multi-time-scale characteristics. The contributions of this study are listed below.

- An energy bus-based matrix-modeling method is proposed, which can be used to formulate steady- and transient-state models of the IES. The modeling process and results are relatively simple.
- A transient-state model that can constitutionally express the multi-time-scale characteristics of the different energy flows is presented.
- Rolling optimization based on the system's transient-state model is used to optimally schedule the multi-energy flows of the IES and compensate for the prediction errors of the RESs and loads. It can accurately track the day-ahead schedule and satisfy supply-demand balances of multi-energy flows to minimize the total operation cost of the IES.

The remainder of this paper is organized as follows. Section 2 describes the matrix-modeling method. Section 3 provides the model parameters. Section 4 describes the coordinated scheduling method. Section 5 provides the case study, and the conclusion is provided in Section 6.

2. Matrix-Modeling Method

2.1. IES Structure Based on Energy Bus

Figure 1 shows the structure and energy flow of a complex IES with various devices. The IES uses the energy from RESs (wind and solar), power, and gas grids and can provide gas, electricity, cooling, and heating for users simultaneously. Any energy flow can be converted into another by using different devices, e.g., a power generation unit (PGU) can consume gas to generate electricity, and an electric chiller can make use of electricity to produce cooling energy. Some energy storage units are also introduced to improve the overall performance of the IES. The existing methods separately analyze and model the balances of the electricity, cooling, and heating, and the modeling processes and results are somewhat complex.

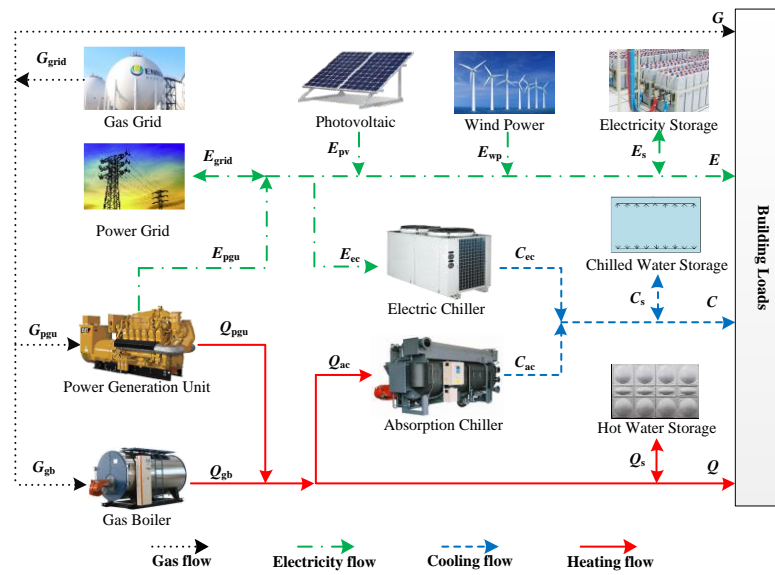


Figure 1. The structure and energy flow of a complex IES.

In this study, an energy bus-based unified modeling method is proposed for the IES. Natural gas, electricity, cooling, and heating are defined as a unified energy vector.

$$e = [G E C Q]^T \tag{1}$$

where G , E , C , and Q represent natural gas, electricity, cooling, and heating, respectively. Then, the IES can be described by an energy bus-based structure, as shown in Figure 2, in which G , E , C , and Q are uniformly expressed as an energy vector e . The balance of the energy vector e can be expressed as

$$e_{grid} + e_{res} + e_{pgu,out} - e_{pgu,in} + e_{gb,out} - e_{gb,in} + e_{ac,out} - e_{ac,in} + e_{ec,out} - e_{ec,in} + e_s = e_{load} \tag{2}$$

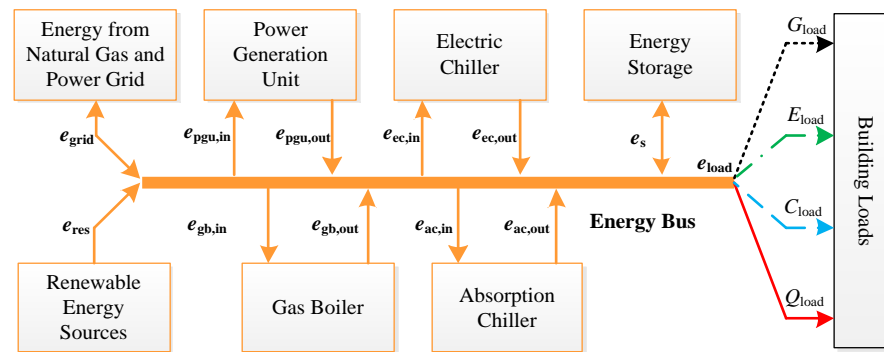


Figure 2. An energy bus-based structure for the IES.

Energy purchased from the gas and power grids is classified as the energy vector e_{grid} , which is generally a controllable vector. WP and PV are classified as the energy input vector e_{res} , whose value needs to be predicted. e_{load} represents the energy output vector of the IES. e_s is the charging ($e_s < 0$) or discharging ($e_s > 0$) vector of the energy storage unit. Its state of charge (SOC) is

$$e_{s,soc}(t + 1) = H_{soc}e_{s,soc}(t) - H_s e_s(t) \tag{3}$$

where H_s is the loss coefficient matrix of the charging and discharging processes. The above ports of the energy bus belong to a single energy input or output vector, which fails to

consider the energy conversion process. Some energy conversion devices or components can acquire any type of energy from the energy bus, and their outputs are injected into the energy bus, e.g., the PGU consumes some gas and returns the converted electricity and heat; the electric chiller inputs some electricity and outputs the corresponding cooling energy. By using an energy bus-based structure, the energy flow analysis can be clarified, which is beneficial in modeling the steady-state and transient-state energy flows of the IES.

2.2. Steady-State Model

If the IES is in the static state, the inputs and outputs of each device are unchanged. The energy conversion process of the devices can be expressed as

$$e_{i,out} = H_i e_{i,in} \tag{4}$$

where $e_{i,out}$ and $e_{i,in}$ are the output and input of the device i , and H_i is the energy conversion matrix of the device i and is defined as

$$H_i = \begin{bmatrix} \eta_{i,G2G} & \eta_{i,E2G} & \eta_{i,C2G} & \eta_{i,Q2G} \\ \eta_{i,G2E} & \eta_{i,E2E} & \eta_{i,C2E} & \eta_{i,Q2E} \\ \eta_{i,G2C} & \eta_{i,E2C} & \eta_{i,C2C} & \eta_{i,Q2C} \\ \eta_{i,G2Q} & \eta_{i,E2Q} & \eta_{i,C2Q} & \eta_{i,Q2Q} \end{bmatrix} \tag{5}$$

where $\eta_{i,x2y}$ represents the conversion efficiency of the energy x to y of the device i . Regarding the PGU, its input is gas and its outputs are electricity and heat. It has two efficiency coefficients: the conversion efficiency of gas to electricity $\eta_{pgu,e}$ and the conversion efficiency of gas to heat $\eta_{pgu,rh}$. Hence, H_{pgu} is

$$H_{pgu} = \begin{bmatrix} 0 & 0 & 0 & 0 \\ \eta_{pgu,e} & 0 & 0 & 0 \\ 0 & 0 & 0 & 0 \\ \eta_{pgu,rh} & 0 & 0 & 0 \end{bmatrix} \tag{6}$$

and $e_{pgu,in}$ is

$$e_{pgu,in} = [\alpha_{pgu} \ 0 \ 0 \ 0]^T \tag{7}$$

where α_{pgu} is the gas input of the PGU. According to the energy conversion mechanism of the gas boiler, absorption chiller, and electric chiller, their energy conversion matrices are defined as

$$H_{gb} = \begin{bmatrix} 0 & 0 & 0 & 0 \\ 0 & 0 & 0 & 0 \\ 0 & 0 & 0 & 0 \\ \eta_{gb} & 0 & 0 & 0 \end{bmatrix} \tag{8}$$

$$H_{ac} = \begin{bmatrix} 0 & 0 & 0 & 0 \\ 0 & 0 & 0 & 0 \\ 0 & 0 & 0 & COP_{ac} \\ 0 & 0 & 0 & 0 \end{bmatrix} \tag{9}$$

$$H_{ec} = \begin{bmatrix} 0 & 0 & 0 & 0 \\ 0 & 0 & 0 & 0 \\ 0 & COP_{ec} & 0 & 0 \\ 0 & 0 & 0 & 0 \end{bmatrix} \tag{10}$$

where COP_{ac} and COP_{ec} are the coefficients of performance of the absorption chiller and electric chiller, respectively. $\eta_{pgu,e}$, $\eta_{pgu,rh}$, η_{gb} , COP_{ac} , and COP_{ec} can be fitted with the operating data of the corresponding devices. They can be represented by constants or polynomials related to the part-load ratio [33]. This means that the models can be linear or nonlinear.

Since most of the conversion devices and components have only one type of input, $e_{i,out}$ can be simplified as

$$e_{i,out} = h_i \alpha_i \tag{11}$$

where h_i is the nonzero column of H_i , and α_i is the input of the device. If purchases of electricity and gas are allowed, e_{grid} can be defined as

$$e_{grid} = [\alpha_{grid,g} \quad \alpha_{grid,e} \quad 0 \quad 0]^T \tag{12}$$

Electricity, chilled water, and hot water storage units are employed in the IES as e_s and are defined as

$$e_s = [0 \quad \alpha_{s,e} \quad \alpha_{s,c} \quad \alpha_{s,h}]^T \tag{13}$$

Hence, the steady-state balance of the energy flow of the IES can be simplified as

$$\begin{aligned} & \begin{bmatrix} 1 \\ 0 \\ 0 \\ 0 \end{bmatrix} \alpha_{grid,g} + \begin{bmatrix} 0 \\ 1 \\ 0 \\ 0 \end{bmatrix} \alpha_{grid,e} + \begin{bmatrix} -1 \\ \eta_{pgu,e} \\ 0 \\ \eta_{pgu,rh} \end{bmatrix} \alpha_{pgu} + \begin{bmatrix} -1 \\ 0 \\ 0 \\ \eta_{gb} \end{bmatrix} \alpha_{gb} + \begin{bmatrix} 0 \\ 0 \\ COP_{ac} \\ -1 \end{bmatrix} \alpha_{ac} + \begin{bmatrix} 0 \\ -1 \\ COP_{ec} \\ 0 \end{bmatrix} \alpha_{ec} \\ & + \begin{bmatrix} 0 \\ \eta_{s,e} \\ 0 \\ 0 \end{bmatrix} \alpha_{s,e} + \begin{bmatrix} 0 \\ 0 \\ \eta_{s,c} \\ 0 \end{bmatrix} \alpha_{s,c} + \begin{bmatrix} 0 \\ 0 \\ 0 \\ \eta_{s,h} \end{bmatrix} \alpha_{s,h} = e_{load} - e_{res} \end{aligned} \tag{14}$$

In the optimal scheduling of the IES, α_{grid} , α_s , and α_i are the decision variables, and they need to be confined to reasonable ranges that are related to the capacities of the devices. Formula (14) can be expanded into the energy flow equilibrium equation in [34] or written as the standard equation constraint form $Ax = b$.

2.3. Transient-State Model

Due to the fluctuations in the RESs and loads, the IES needs to continually adjust the set points (inputs) of the devices. After each adjustment, the system takes a period of time to enter the steady state. For electricity and gas, the steady state can be achieved quickly, while a long time (a few minutes to tens of minutes) is required for the energy flows of cooling and heat. In the rolling optimization of the IES, the cooling and heat are mostly in an unsteady state, so it is necessary to use a transient model of the energy flow. The details will be discussed in this subsection.

For energy conversion devices, the transient values of their output energy flow depend on their state vectors x_i , and the transient model can be represented as

$$\begin{aligned} \dot{x}_i &= A_i x_i + B_i e_{i,in} \\ e_{i,out} &= C_i x_i \end{aligned} \tag{15}$$

where $A_i \in \mathbb{R}^{m \times m}$ is the state matrix of the device i , $B_i \in \mathbb{R}^{m \times 4}$ is the input matrix, and $C_i \in \mathbb{R}^{4 \times m}$ is the output matrix. In rolling optimization, the corresponding discrete-time models of the devices are required. Let $T_s \in \mathbb{R}$ denote the sampling period, and the set points of the devices can hold at least one sampling period, i.e., $e_{i,in}(k)$ remains constant between kT_s and $(k + 1)T_s$. Hence, model (15) can be discretized as follows:

$$\begin{aligned} x_i(k) &= L_i x_i(k-1) + R_i e_{i,in}(k) \\ e_{i,out}(k) &= C_i x_i(k) \end{aligned} \tag{16}$$

with

$$L_i = \exp(A_i T_s), R_i = \int_0^{T_s} \exp(A_i t) dt B_i \tag{17}$$

where $L_i \in \mathbb{R}^{m \times m}$ and $R_i \in \mathbb{R}^{m \times 4}$ are the state matrix and input matrix of the discrete-time model of the device i in a fixed sampling period T_s , respectively. Through (16), it is obtained that

$$\begin{aligned} x_i(k) &= L_i^k x_i(0) + L_i^{k-1} R_i e_{i,in}(1) + \dots + R_i e_{i,in}(k) \\ e_{i,out}(k) &= C_i x_i(k) \end{aligned} \tag{18}$$

This shows the transient energy output $e_{i,out}$ at any sampling point. On this basis, the energy supply and demand can achieve a strict balance and the set point optimization for any energy flow can be implemented in the same rolling cycle.

In this study, the state vectors of the PGU, gas boiler, absorption chiller, and electric chiller are their output vectors, i.e., $C_i = I$. This means that the transient conversion of the natural gas, electricity, cooling, and heat energy flows has inertial characteristics, which mainly exist in the transfer of a certain energy flow. For the cooling and heating processes, the chiller and PGU must bring the cooling and heating media to certain temperatures, and their energy outputs vary with the temperatures of the media. The transient state of electricity or gas changes very quickly and can be approximated as an inertial element. Hence, the state matrix can be expressed as

$$A_i = \begin{bmatrix} -1/\tau_{i,g} & 0 & 0 & 0 \\ 0 & -1/\tau_{i,e} & 0 & 0 \\ 0 & 0 & -1/\tau_{i,c} & 0 \\ 0 & 0 & 0 & -1/\tau_{i,h} \end{bmatrix} \tag{19}$$

where $\tau_{i,g}$, $\tau_{i,e}$, $\tau_{i,c}$, and $\tau_{i,h}$ are the gas, electricity, cooling, and heat inertia time coefficients of device i . The input matrix is represented as

$$B_i = -A_i H_i \tag{20}$$

The transient-state model of device i is

$$e_{i,out}(k) = L_i^k e_{i,out}(0) + L_i^{k-1} R_i e_{i,in}(1) + \dots + R_i e_{i,in}(k) \tag{21}$$

with

$$L_i = \begin{bmatrix} \exp(-T_s/\tau_{i,g}) & 0 & 0 & 0 \\ 0 & \exp(-T_s/\tau_{i,e}) & 0 & 0 \\ 0 & 0 & \exp(-T_s/\tau_{i,c}) & 0 \\ 0 & 0 & 0 & \exp(-T_s/\tau_{i,h}) \end{bmatrix} \tag{22}$$

$$R_i = (I - L_i) H_i \tag{23}$$

It is clear that the transient output at a specified time kT_s can be calculated via the input sequence $u(0), \dots, u(k)$. If the sampling time T_s is sufficiently greater than the inertia time τ , we can obtain

$$L_i \rightarrow \mathbf{0}, R_i \rightarrow H_i \tag{24}$$

and the transient-state model can be degraded into the steady-state model.

3. Model Parameters

3.1. Steady-State Model Parameters

Typically, the conversion efficiency η can use a constant in the optimal scheduling, as shown in Table 1 [5]. However, in the IES with RESs, the fluctuations in the RESs often cause the devices to run in off-design conditions. The conversion efficiency of the boiler is almost linear, while the electric chiller can work periodically. Hence, η_g and COP_{ec} can use constant coefficients.

Table 1. The constant efficiency of the energy converters.

Converter	Efficiency
PGU	$\eta_{pgu,e} = 0.3$ $\eta_{pgu,th} = 0.4$
Gas boiler	$\eta_g = 0.8$
Absorption chiller	$COP_{ac} = 0.7$
Electric chiller	$COP_{ec} = 3$

In this study, $\eta_{pgu,e}$ is fitted with the operating data of the real generator, and COP_{ac} is fitted with the simulation data in [33]. The polynomial fitting results with 95% confidence bounds are as follows:

$$\eta_{pgu,e} = \begin{cases} 0 & PIR_{pgu} = 0 \\ -2.799PIR_{pgu}^4 + 9.276PIR_{pgu}^3 - 11.44PIR_{pgu}^2 + 6.454PIR_{pgu} - 1.181 & PIR_{pgu} \geq 0.3288 \end{cases} \quad (25)$$

$$COP_{ac} = 1.386PIR_{ac}^4 - 1.943PIR_{ac}^3 - 0.2784PIR_{ac}^2 + 1.214PIR_{ac} + 0.4216 \quad (26)$$

where PIR is the part-input ratio and is defined as

$$PIR = \frac{v_{in}}{v_{in,rc}} \quad (27)$$

where v_{in} is the input value of the energy conversion device, and $v_{in,rc}$ is the input value in the rated condition. Considering that the conversion is inefficient if the PGU runs under light-load conditions, we set $PIR_{pgu} \geq 0.4$ in the experiment. $\eta_{pgu,e}$ can be calculated via [33]

$$\eta_{pgu,th} = 0.8(1 - \eta_{pgu,e}) \quad (28)$$

The efficiency and fitting curves are plotted in Figures 3 and 4. The R-squared values of $\eta_{pgu,e}$ and COP_{ac} are 0.9998 and 0.9771, respectively. The nonlinear parameter provides an exact description of each device under the off-design condition.

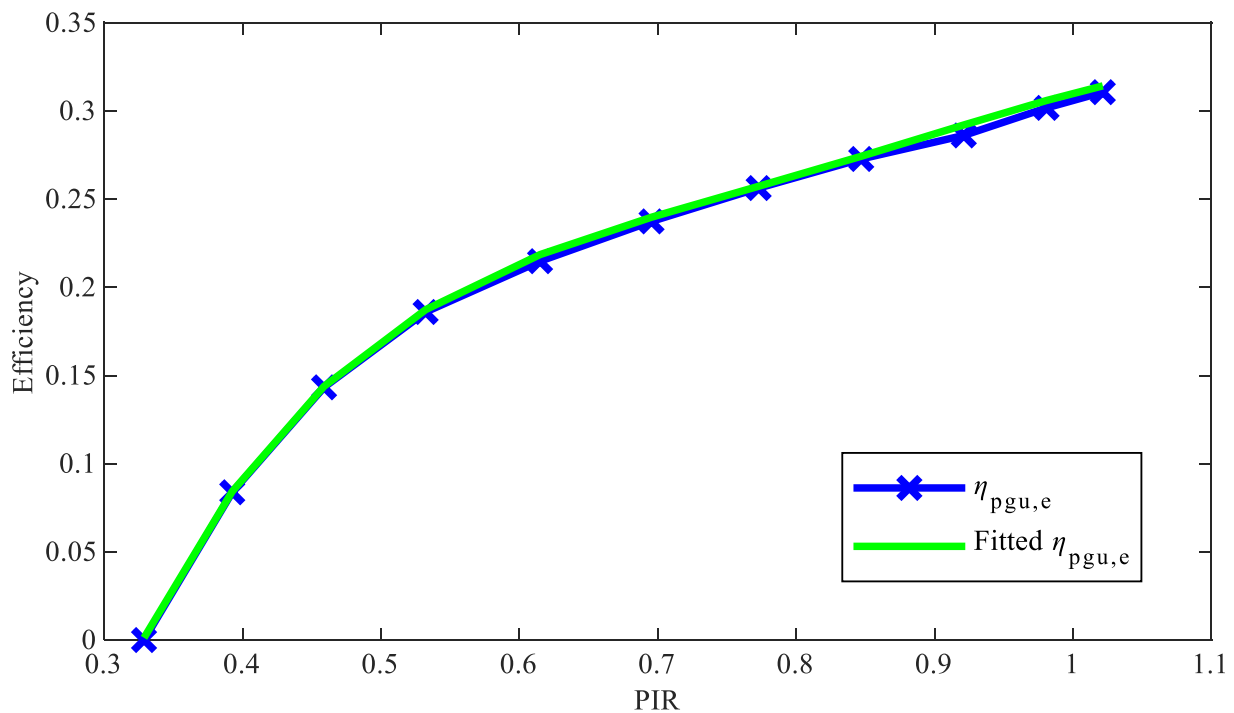


Figure 3. The efficiency curves of the PGU.

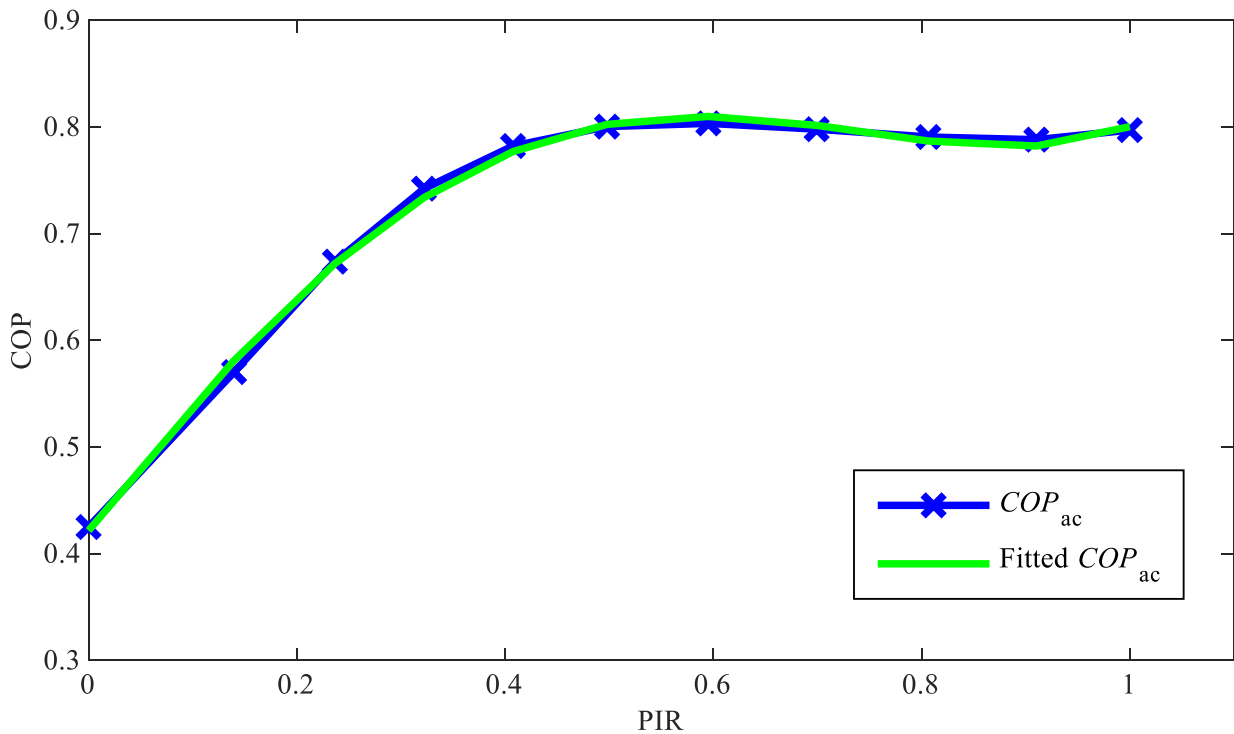


Figure 4. The COP curves of the absorption chiller.

3.2. Transient-State Model Parameters

The transient-state model parameters need to be identified using the dynamic process data. Considering that the inertia time coefficients are mainly impacted by the machine and thermodynamic characteristics and are less affected by the running time and input energy, we identify each coefficient as a constant using the System Identification Tool in MATLAB. The PGU converts gas into electricity and heat, so its electricity and heat inertia time constants need to be identified. We increase the gas input from 52.034 kW to 59.714 kW at 203 s and to 67.727 kW at 1192 s, and we obtain $\tau_{pgu,e}$ and $\tau_{pgu,h}$ as 0.382 and 125. The real outputs and the transient model outputs are shown in Figure 5. Due to the use of a constant temperature control, the heat output has some fluctuations. The transient model of the PGU can be used to reasonably simulate the dynamic process of its electricity and heat. For the absorption chiller, we identify $\tau_{ac,c}$ using the dynamic simulation data in [35]. The input of the absorption chiller is increased at 100 s. The result is shown in Figure 6, in which it can be seen that there is a small time delay between the output and input of the absorption chiller. It can be expressed as a modified model:

$$e_{ac,out}(k) = L_{ac}^k x_{ac}(0) + \sum_{j=1}^k L_{ac}^{k-j} R_{ac} e_{ac,in}(j - \mu) \tag{29}$$

with

$$L_{ac} = \begin{bmatrix} 0 & 0 & 0 & 0 \\ 0 & 0 & 0 & 0 \\ 0 & 0 & 0 & 0 \\ 0 & 0 & 0 & -1/71.429 \end{bmatrix}, \mu = 15 \tag{30}$$

where μ is a time delay coefficient. This can simulate the dynamic process of the absorption chiller accurately, as shown by the green dashed line in Figure 6. For ease of use in rolling optimization, the time delay is ignored. The inertia time coefficient $\tau_{ac,c}$ is 80 and the corresponding result is plotted as the red dotted line in Figure 6; it also models the dynamic process effectively.

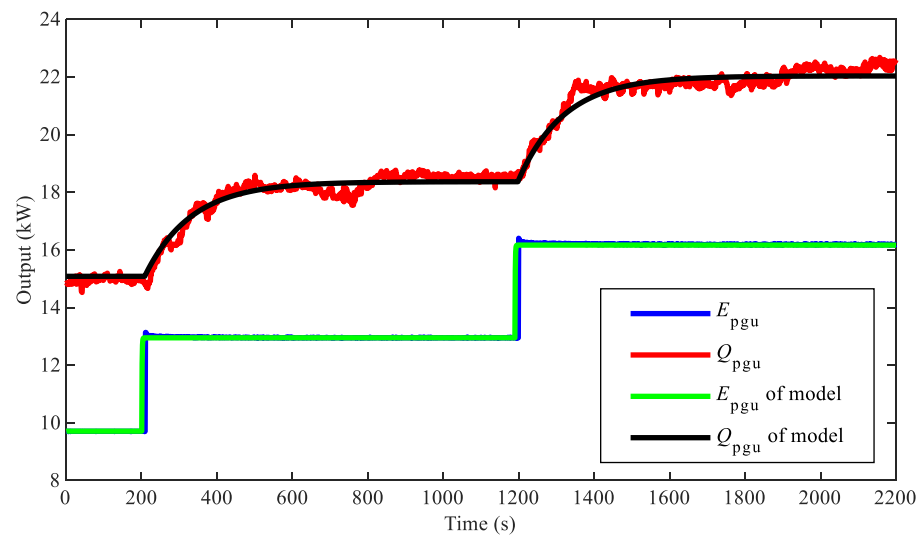


Figure 5. The transient process of the PGU.

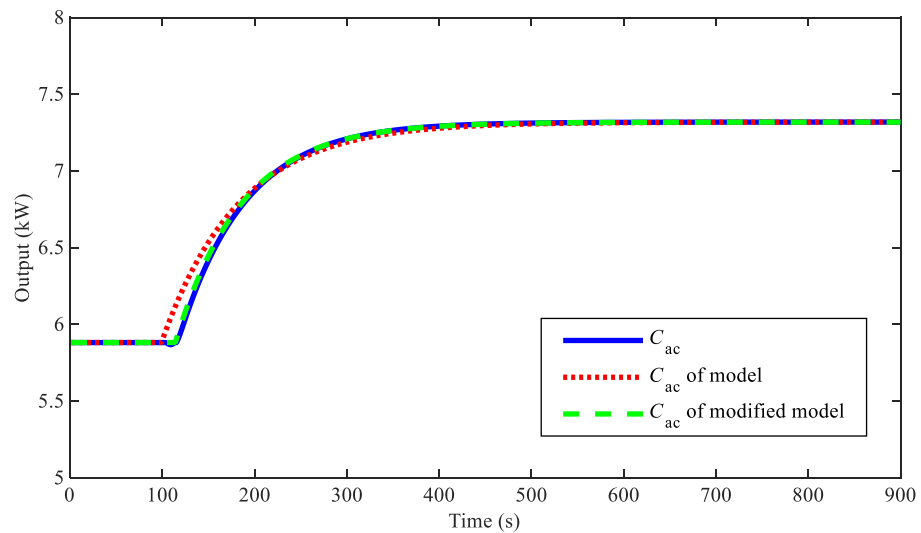


Figure 6. The transient process of the absorption chiller.

4. Optimal Scheduling of IES

Since the RESs and user loads have the properties of periodicity and randomness, the optimal scheduling of the IES consists of two stages or time scales, including day-ahead scheduling and rolling optimization. The schematic diagram is shown in Figure 7. Day-ahead scheduling runs once a day and determines the optimal hourly set point of each device based on the forecast hourly RES outputs and multiple energy demands in the next 24 h. It can coordinate the scheduling of devices, such as the PGU, absorption chiller, gas boiler, electric chiller, energy storage unit, and so on, to minimize the operating cost of the IES while satisfying the energy supply–demand balance and the device constraints. The hourly electricity and gas consumption plans need to be sent to the scheduling centers of the power grid and gas grid for day-ahead scheduling purposes. Due to errors in the predicted data, rolling optimization is employed to correct the day-ahead scheduling scheme. Its task is to ensure that the amounts exchanged with the power and gas grids follow the day-ahead schemes as much as possible while satisfying the energy supply–demand balance and the device constraints. However, the correction will cause some unplanned costs to be incurred, which can be considered in the rolling optimization. The details of the optimization model will be described in the following sections.

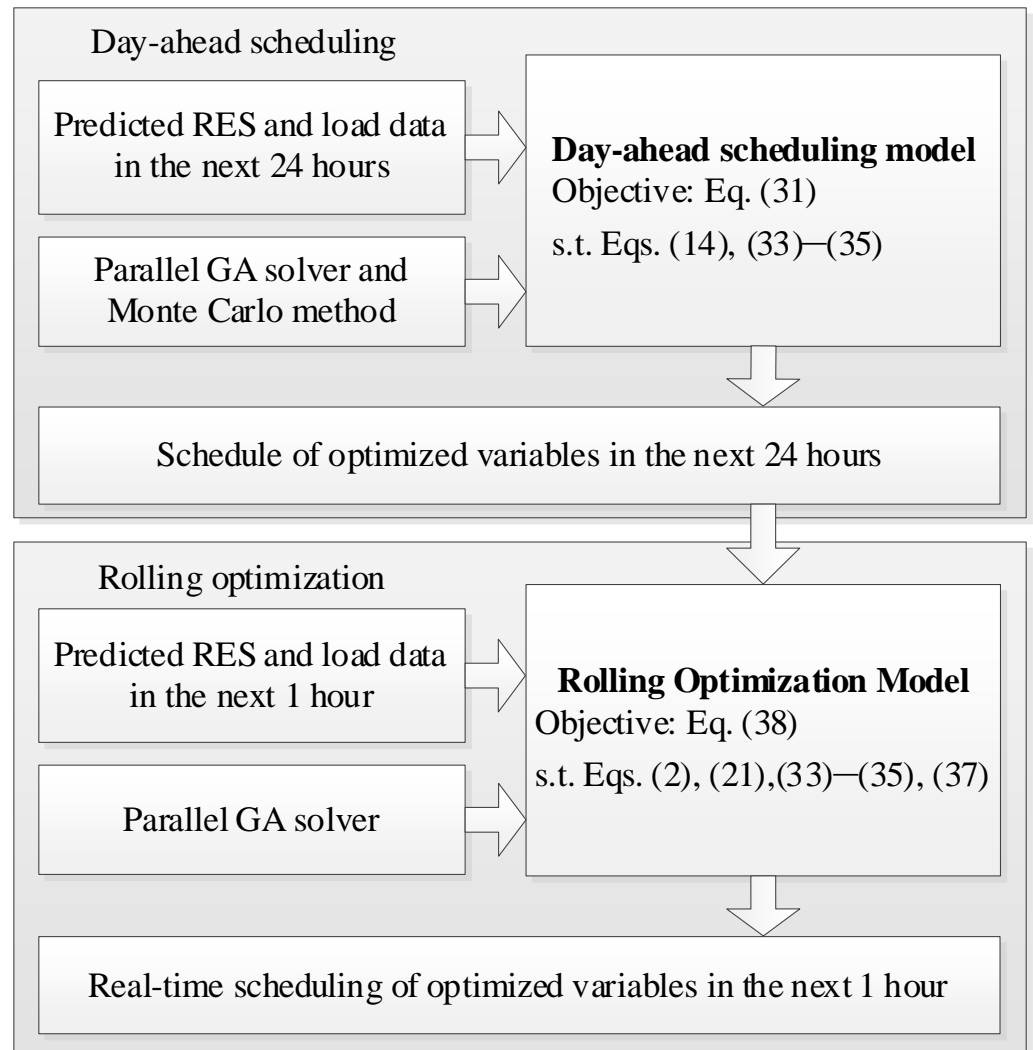


Figure 7. The schematic diagram of optimal scheduling for the IES.

4.1. Day-Ahead Optimization

In day-ahead scheduling, we expect that the total daily cost can be minimized by optimizing the hourly set points of the devices. The day-ahead optimization interval T_d is 1 h. Considering the stochastic fluctuations in the RESs and the users' demands, the objective function is defined as

$$\min \text{COST} = E \left[\sum_{t=1}^{24} \mathbf{p}(t)^T \mathbf{e}_{\text{grid}}(t) \right] \tag{31}$$

where t ($t \in [1, 24]$) denotes the t -th hour of a day, and $\mathbf{p}(t)$ is the price vector of the energy purchased from the gas and power grids in period t . It is expressed as

$$\mathbf{p}(t) = [p_G(t) \quad p_E(t) \quad 0 \quad 0]^T \tag{32}$$

where $p_G(t)$ and $p_E(t)$ are the prices of gas and electricity in period t , respectively.

The day-ahead optimization must satisfy the balance constraint of the energy flow expressed in (14). Each energy converter or storage unit must run within its capacity; therefore, each decision variable $\alpha_i(t)$ must meet the following constraint:

$$0 \leq \alpha_i(t) \leq \alpha_{i,rc} \tag{33}$$

where $\alpha_{i,rc}$ is the input of the device i in the rated condition. The SOC of the energy storage unit should be subject to the following constraints:

$$\begin{aligned} 0 \leq \alpha_{s,soc}(t+1) &= \eta_{soc}\alpha_{s,soc}(t) - \eta_s\alpha_s(t) \leq \alpha_{s,soc,max}, \\ 0 \leq \alpha_{s,soc}(t) &\leq \alpha_{s,soc,max} \end{aligned} \tag{34}$$

where $\alpha_{s,soc,max}$ is the maximum SOC of the energy storage unit. In addition, to ensure the same flexibility of the energy storage on each scheduling day, the initial and final SOCs should be equal:

$$\alpha_{s,soc}(1) = \alpha_{s,soc}(25) \tag{35}$$

Finally, the day-ahead optimization model can be summarized as follows:

$$\begin{aligned} \text{Objective function:} & \text{Equation (31)} \\ \text{Subject to:} & \text{Equations (14), (33)–(35)} \end{aligned} \tag{36}$$

In summer conditions, the boiler and heat storage unit do not operate, so the decision variables include $\alpha_{grid,g}(t)$, $\alpha_{grid,e}(t)$, $\alpha_{pgu}(t)$, $\alpha_{ac}(t)$, $\alpha_{ec}(t)$, $\alpha_{s,e}(t)$, and $\alpha_{s,c}(t)$. Similarly, the decision variables include $\alpha_{grid,g}(t)$, $\alpha_{grid,e}(t)$, $\alpha_{pgu}(t)$, $\alpha_{gb}(t)$, $\alpha_{s,e}(t)$, and $\alpha_{s,h}(t)$ in winter conditions. For some specific problems, the decision variables need to be selected according to the structure and operating mode, because some decision variables may be unnecessary. Due to the nonlinear of the PGU and absorption chiller models, (36) is a nonlinear optimization problem.

4.2. Rolling Optimization

Rolling optimization is designed for the real-time scheduling of devices. By using the real-time predicted data of the RESs and loads, it can correct the errors of the day-ahead prediction. The RESs' outputs and the electricity load fluctuate at the time scale of several minutes. Thus, the scheduling of the devices is executed every 5–15 min [25,27]. The shorter the time interval used, the higher the computational accuracy, but also the computational complexity. Since this study employs a parallel genetic algorithm that includes multi-energy flow balance constraints and has the objective of optimal economic scheduling, the rolling interval T_{roll} is set as 5 min and every optimization covers a time window of 1 h (12 time intervals). The optimization results of the first-time interval are used to schedule the devices, and the results of other intervals are used for reference only. After completing a rolling optimization cycle, the time window moves forward by one interval. In this case, the cooling and heat flows are not able to reach a steady state. It is necessary to use the transient-state IES model in the rolling optimization. The sampling period T_s is set as 1 s, and the output of the transient-state model in one rolling cycle can be calculated via

$$e_{i,out}(j) = \frac{T_s}{T_{roll}} \sum_{k=300j}^{300j+299} e_{i,out}(k) \tag{37}$$

where j ($j \in [1, 288]$) denotes the j -th 5 min of a day.

Rolling optimization aims to ensure that the actual electricity and natural gas exchanges between the IES and the grids follow the day-ahead schedules as closely as possible while minimizing the operating cost. The objective function of rolling optimization can be defined as

$$\min Obj(r) = \sum_{j=r}^{r+11} \left(\gamma^T |e_{grid,d}(j) - e_{grid,r}(j)| + p(j)^T e_{grid}(j) \right) \tag{38}$$

where r ($r \in [1, 288]$) denotes the r -th rolling time interval; $e_{grid,d}$ and $e_{grid,r}$ represent the day-ahead and real-time scheduling schemes of the grids, respectively; and γ is the

weighting vector of the gas, power, cooling, and heat grids. Regarding the power grid, it is generally expected that the IES can purchase and sell electricity as planned, so γ is

$$\gamma = [0 \quad 1 \quad 0 \quad 0]^T \quad (39)$$

Similarly, rolling optimization must meet the constraints in (2) and (33)–(35), in which the time interval is 5 min and $e_{i,\text{out}}(j)$ is calculated using (21) and (37).

Finally, the rolling optimization problem can be summarized as follows:

$$\begin{aligned} &\text{Objective function: Equation (38)} \\ &\text{Subject to: Equations (2), (21), (33)–(35), (37)} \end{aligned} \quad (40)$$

All decision variables include $\alpha_{\text{grid,g}}(j)$, $\alpha_{\text{grid,g}}(j)$, $\alpha_{\text{pgu}}(j)$, $\alpha_{\text{gb}}(j)$, $\alpha_{\text{ac}}(j)$, and $\alpha_{\text{ec}}(j)$, while the variables $\alpha_{\text{s,e}}(j)$, $\alpha_{\text{s,c}}(j)$, and $\alpha_{\text{s,h}}(j)$ refer to the day-ahead optimization results.

4.3. Solving Algorithm

The day-ahead and rolling optimization models presented in (36) and (40) are nonlinear optimization problems with complex constraints. They can be solved by using some heuristic optimization algorithms, such as the GA and PSO [36,37]. In this study, the parallel GA is used to solve these problems.

5. Case Study

5.1. Basic Parameter

In this study, a hypothetical IES is constructed to assess and verify the performance of the proposed day-ahead and rolling optimization methods. This system works in summer conditions and provides electricity and cooling for all users. It consists of a PGU, an absorption chiller, an electric chiller, electricity, and chilled water storage units, WP, and PV, and it can purchase electricity and natural gas from the main grids. The IES is designed according to the typical electricity and cooling demands, and its device parameters are listed in Table 2.

Table 2. The device parameters of the IES.

Device	Capacity
PGU	100 kW
WP	150 kW
PV	50 kW
Absorption chiller	150 kW
Electric chiller	150 kW
Electricity storage	300 kWh
Chilled water storage	300 kWh

The curves of the electricity and cooling load forecast data are shown in Figure 8 (green solid line) and Figure 9 (red solid line), respectively. The curves of the power output forecast data for PV and WP are shown in Figure 10 (green solid line) and Figure 11 (green solid line), respectively. Considering the prediction errors between the forecast data and the actual source/load data, and assuming that the prediction errors follow a normal distribution $(\mu, 0.1\mu)$, the Monte Carlo method is used to generate 100 sets of source/load data samples, as shown in Figures 8–11. One set of samples is selected as the real source/load data (test sample) to evaluate the results of day-ahead stochastic optimization and deterministic optimization.

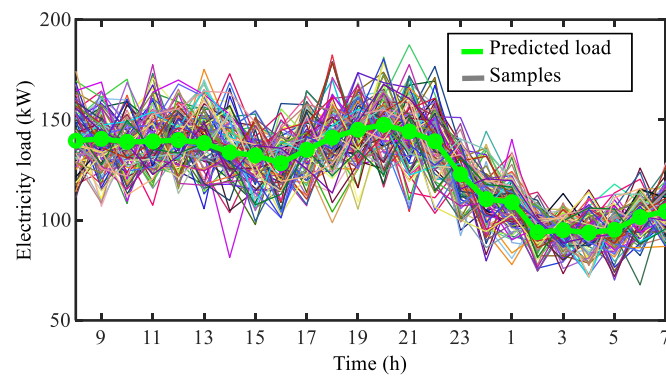


Figure 8. Electricity load forecast curve and samples.

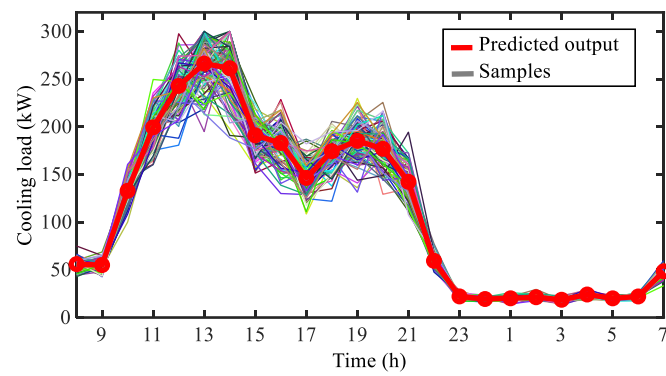


Figure 9. Cooling load forecast curve and samples.

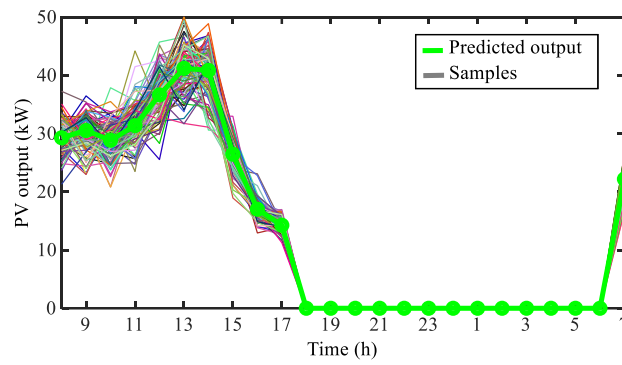


Figure 10. PV power output forecast curve and samples.

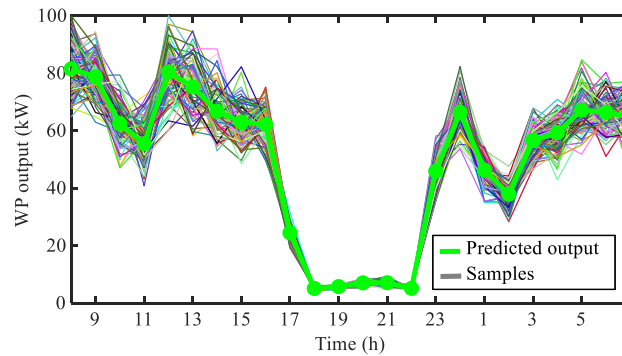


Figure 11. WP power output forecast curve and samples.

In rolling optimization, probability sampling is applied to the test samples selected for day-ahead optimization to obtain the forecast data and actual fluctuation data for rolling optimization. The probability distributions are $(\mu, 0.05\mu)$ and $(\mu, 0.02\mu)$, respectively. Specifically, the variance in the forecast data in rolling optimization is smaller than that in the day-ahead forecast data, indicating that they have smaller prediction errors. The real-time forecast data and actual data for the electricity load, cooling load, WP, and PV in rolling optimization are shown in Figures 12–15 respectively.

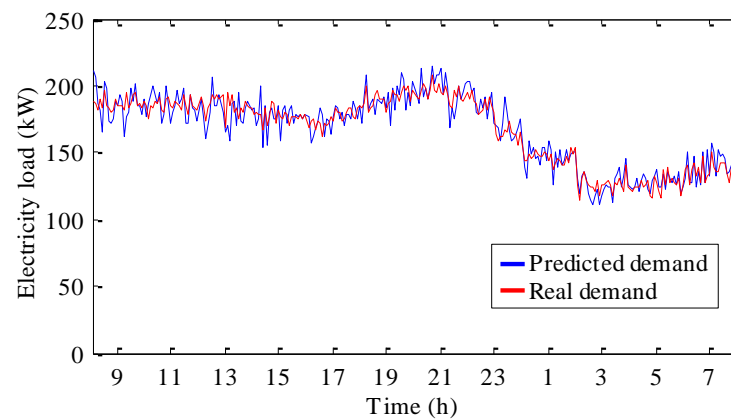


Figure 12. Electricity load real-time forecast curve.

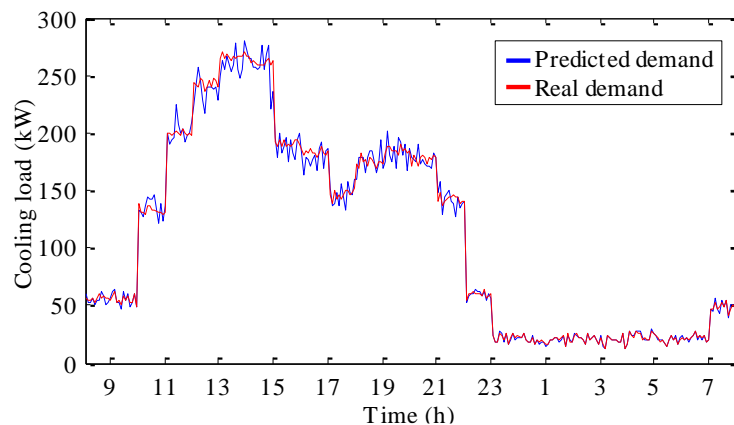


Figure 13. Cooling load real-time forecast curve.

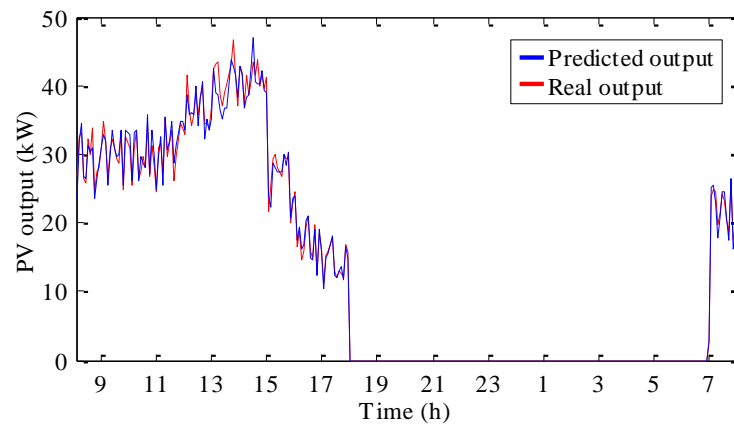


Figure 14. PV output real-time forecast curve.

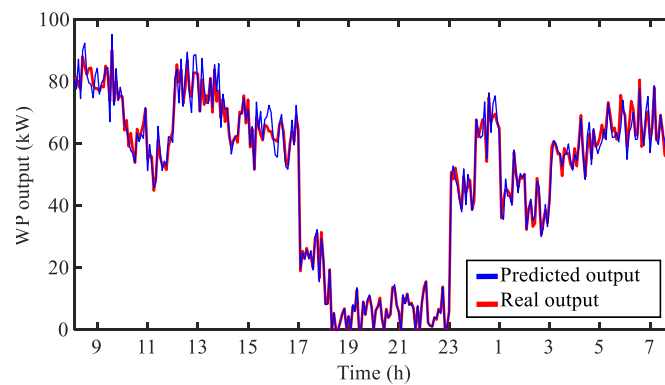


Figure 15. WP output real-time forecast curve.

5.2. Analysis of Day-Ahead Optimization Results

To compare the performance differences between the day-ahead stochastic optimization and deterministic optimization methods and to verify the adaptive ability of stochastic optimization to predict errors, we provide comparative simulation results for day-ahead stochastic optimization and deterministic optimization in the grid-connected mode that forbids the selling of electricity, as shown in Table 3. When testing the prediction data and samples, the input/output of the electricity and cold storage devices are based on the scheduling results of the two optimization methods, while the set points of the other devices need to be recalculated based on the test data. In the sample test, assuming that the source and load data are fully known, the set points of the PGU, absorption chiller, and other devices are calculated, along with the operating costs. The objective function of stochastic optimization is the expected minimum operating cost across multiple samples, while that of deterministic optimization is the minimum operating cost based on the RES and load prediction data. Therefore, when testing with prediction data, where the errors in the RES and load prediction data are zero, the results of deterministic optimization will inevitably be better than those of stochastic optimization. When testing with a set of random samples, where there are some errors in the RES and load prediction data, the results of stochastic optimization are likely to be better than those of deterministic optimization. In random sample testing, stochastic optimization reduces the total daily cost by 1.48% compared to deterministic optimization, reflecting the stronger adaptability of stochastic optimization to prediction errors. Without rolling optimization on the test samples, the IES experiences an over-supply phenomenon. The use of storage devices to store excess electricity, heat, and cold energy can be implemented to revise the scheduling scheme.

Table 3. Comparative simulation results of day-ahead stochastic optimization and deterministic optimization.

Optimization Strategy	Objective Function Value	Prediction Data Testing	Sample Testing
Day-ahead stochastic optimization (CNY)	1568.5	1542.2	1606.0
Day-ahead deterministic optimization (CNY)	1511.9	1511.9	1630.2

Without revision, when using all samples of RES and load data to test the two methods, the results, as shown in Figure 16, indicate significant fluctuations in the minimum operating costs for both methods. When the actual output of the RESs is smaller than predicted and the load demands are higher, the operating cost exceeds the expected values; conversely, the costs are below the expectations when the conditions are reversed. It is evident from the majority of the sample tests that the minimum operating costs in stochastic optimization are consistently lower than those in deterministic optimization, demonstrating its stronger adaptability to prediction errors in the RES and load data.

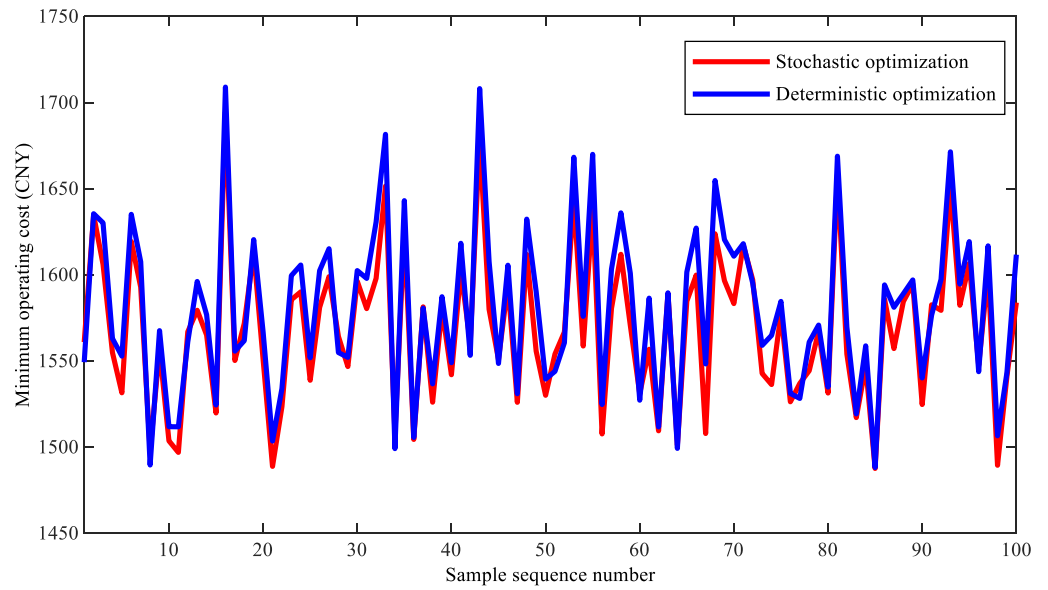


Figure 16. Comparison results of all samples.

Regarding the sample tests, the revised electricity scheduling results for the two methods are shown in Figures 17 and 18. Both methods feature the same power generation for the WP, PV, and electricity demand, with the PGU operating during periods of higher electricity prices and the storage devices effectively performing peak shaving. From 23:00 to 07:00 on the next day, when the purchase price of electricity is lower, it is more economical for the system to buy electricity from the power grid. Comparing the hourly output plans of the devices, it is seen that those of the PGU for the two methods are different. At 12:00, in the stochastic optimization method, the PGU has higher output, whereas, in the deterministic optimization method, it ceases operation; at other times, in the deterministic optimization method, the output of the PGU is slightly higher than in the stochastic optimization method. From 18:00 to 23:00, when the power generation of WP and PV is minimal and the grid electricity prices are higher, the stochastic optimization method uses the PGU and the electricity storage unit to supply electricity to the users, whereas the deterministic optimization method needs to purchase a small amount of electricity from the power grid, thus incurring slightly higher operating costs.

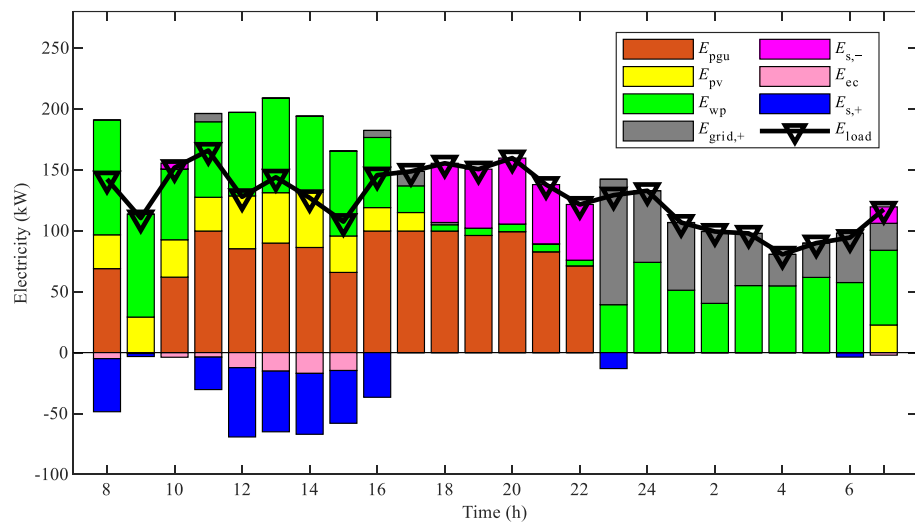


Figure 17. Revised day-ahead stochastic optimization scheduling results for electricity.

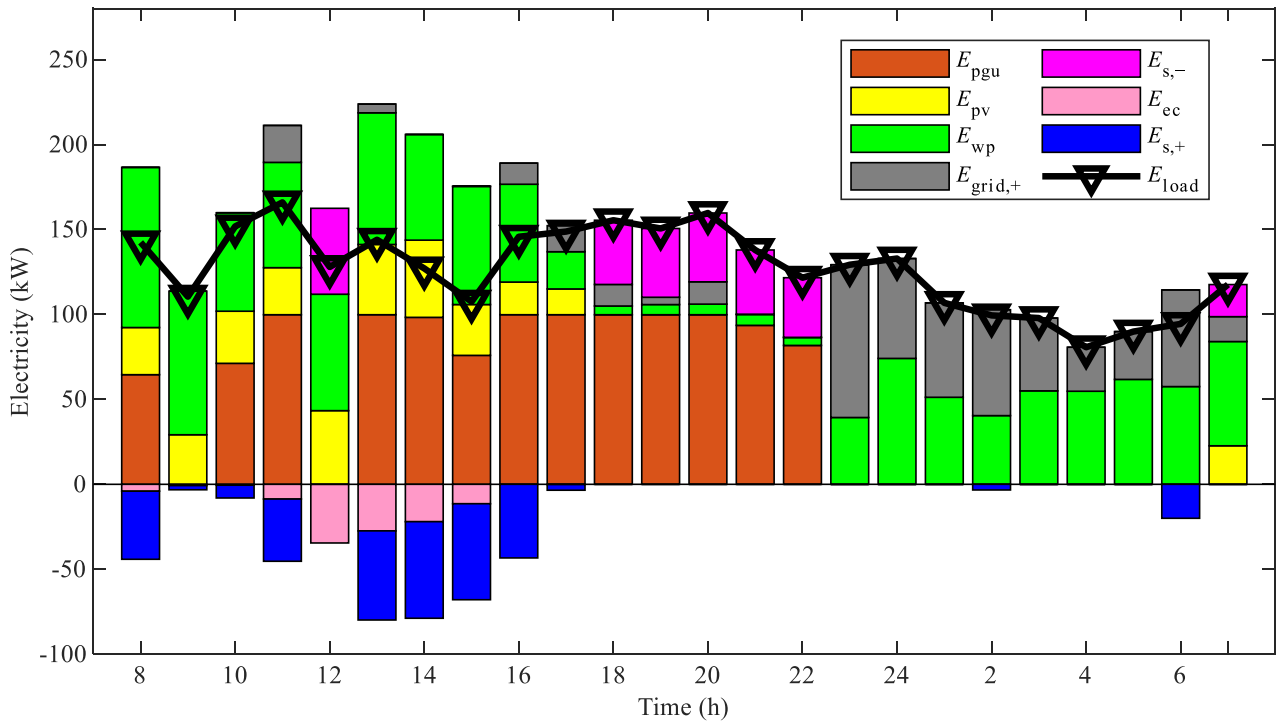


Figure 18. Revised day-ahead deterministic optimization scheduling results for electricity.

The cooling energy scheduling results for the two methods are shown in Figures 19 and 20. From 8:00 to 23:00, both methods primarily use the absorption chiller for cooling. In the deterministic optimization method, the PGU operates for one hour less, requiring the chilled water storage unit and the electric chiller to supply more cooling energy, which leads to an increased operating cost. From 23:00 to the next day at 8:00, the two methods utilize the cold storage unit for cooling.

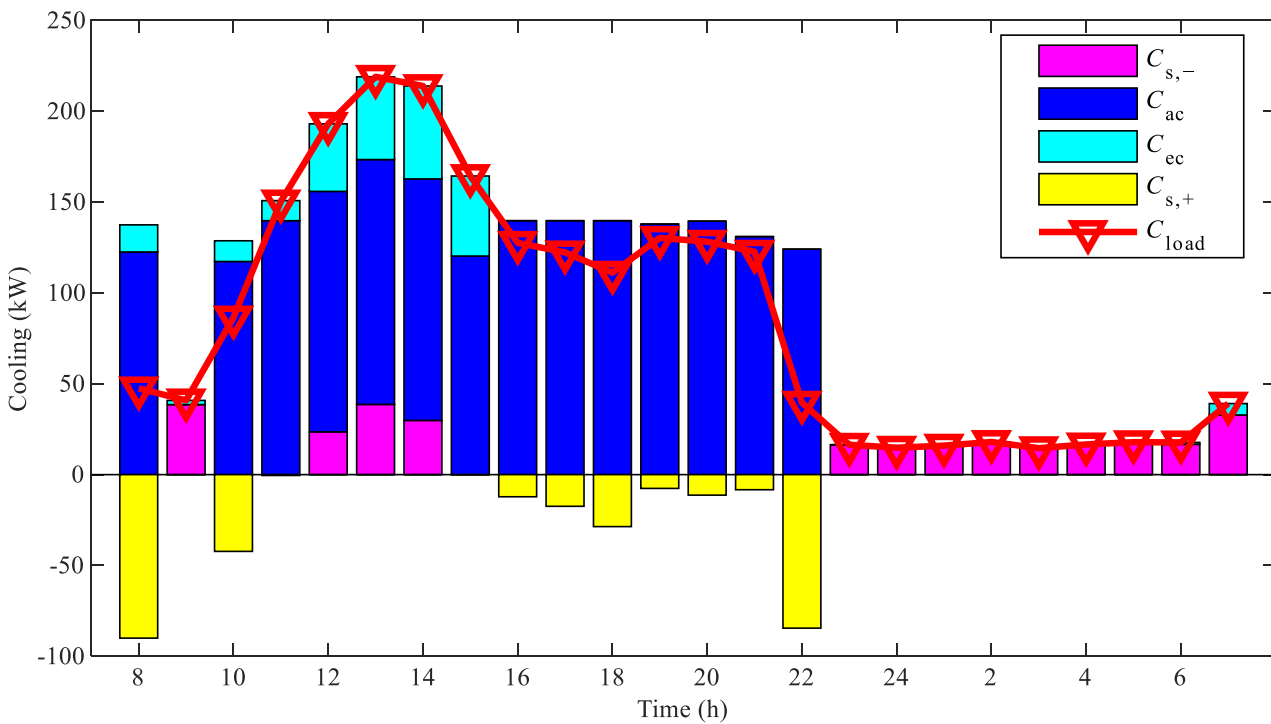


Figure 19. Revised day-ahead stochastic optimization scheduling results for cooling energy.

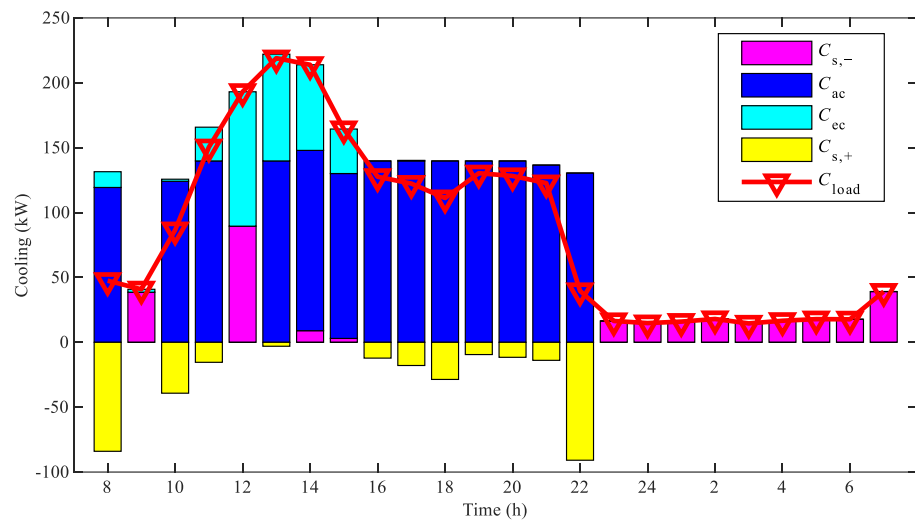


Figure 20. Revised day-ahead deterministic optimization scheduling results for cooling energy.

5.3. Analysis of Rolling Optimization Results

In this case, the rolling optimization strategy revises the day-ahead scheduling scheme on the real-time RES and load prediction data, with the objective function defined as the deviation in the electricity purchase scheme and the operating cost for the upcoming hour. The rolling optimization results based on the comparison of the day-ahead stochastic and deterministic optimization schemes are shown in Figure 21. Rolling optimization cannot be implemented when the PGU is turned off, and the results of the two rolling optimization methods are primarily concentrated between 8:00 and 22:00. Rolling optimization based on the day-ahead stochastic optimization scheme has a smaller objective function value, and the standard deviation of its objective value is reduced by 42.79% compared to that of rolling optimization based on the deterministic optimization scheme, indicating smaller revisions to the devices and stronger adaptability to prediction errors. The maximum objective function values of the rolling optimization method based on the day-ahead stochastic optimization scheme and the rolling optimization method based on the deterministic optimization scheme are 40.95 and 70.52, respectively, and their minimum values are 0, indicating that the former has a stronger ability to deal with anomalies. There are still some prediction errors in the RES and load data during rolling optimization, and actual supply and demand imbalances exist. Therefore, in actual operation, the use of storage devices to store excess electricity and cooling energy ensures a real-time supply and demand balance.

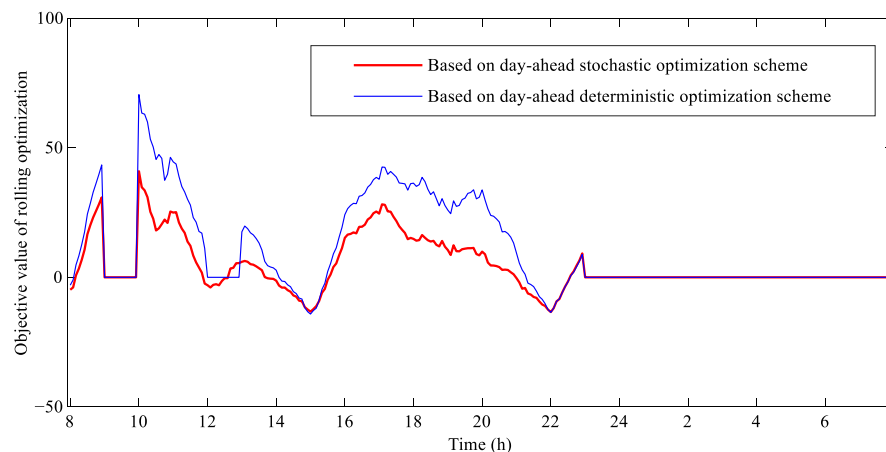


Figure 21. Comparison of results of two rolling optimization methods.

Figures 22 and 23 present the rolling optimization scheduling results for electricity and cooling energy, revised with the use of energy storage units. From 8:00 to 23:00, during each rolling optimization interval, the IES purchases less electricity from the grid, primarily adjusting the power output of the PGU to respond to the stochastic fluctuations in renewable power generation and the electrical load. It also regulates the input/output of the electricity storage unit to achieve an energy supply–demand balance, thereby reducing the fluctuations in the electricity purchases and operating costs. From 23:00 to 8:00 on the next day, when the PGU is not operating, the IES primarily adjusts the amount of electricity purchased to maintain the supply–demand balance. Similarly, in terms of the cooling supply, the system adjusts the real-time output of the electric chiller and the input/output of the chilled water storage unit to ensure a stable supply of cooling energy.

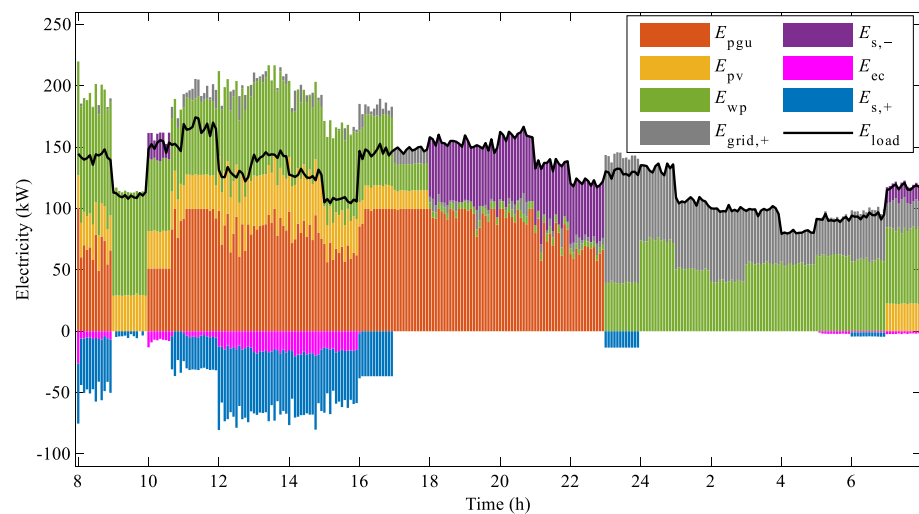


Figure 22. Revised rolling optimization scheduling results for electricity.

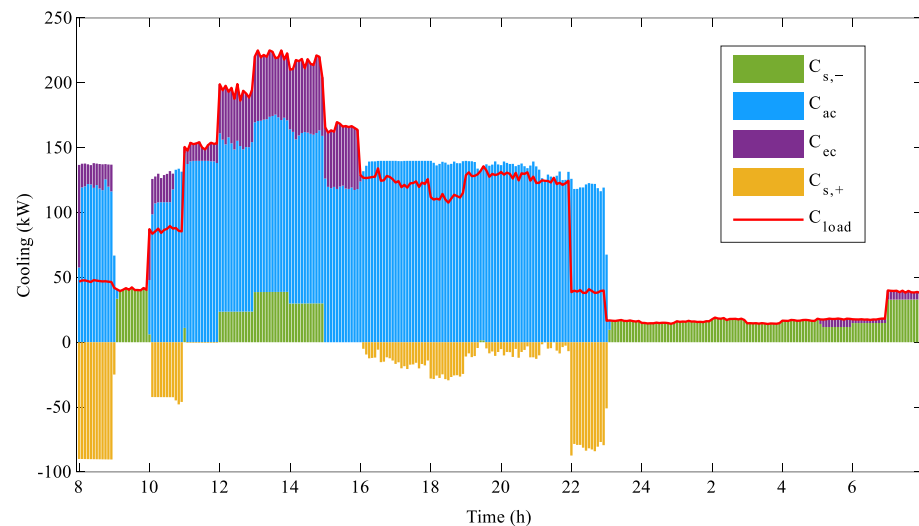


Figure 23. Revised rolling optimization scheduling results for cooling energy.

6. Conclusions

This study proposes the concept of an energy bus for IESs, defining natural gas, electricity, cooling, and heating as a unified energy vector. Thus, the structure of the IES can be represented as a structural diagram based on the energy bus. The energy transfers and coupling relationships between the devices are equivalent to the interaction between the device and the energy bus so that the matrix model is quickly established to characterize the energy balance relationships of the multiple energy flows in the system.

On this basis, the steady-state matrix model and transient-state matrix model are built. In the steady-state model, the definitions of the device input vector and energy conversion coefficient matrix are shown first, and then, the equilibrium equation of the gas, electricity, cooling, and heat vectors is established, which can be directly transformed into the standard form of the equation constraints for the optimization problem. As for the transient-state model, considering the difficulty in solving the optimization problem, the first-order inertial time constant matrix is used to represent the dynamic characteristics of the device, and then a method to obtain the transient-state matrix models of the devices is proposed. By using curve fitting and system identification methods, the parameters of the steady-state and transient-state matrix models of typical devices are obtained, and the fitting results are good.

The steady-state and transient-state matrix models established in this study are applied for day-ahead stochastic optimization and rolling optimization, so as to obtain day-ahead hourly scheduling and an intraday 5 min scheduling correction scheme. The simulation results show that stochastic optimization reduces the total daily cost by 1.48% compared to deterministic optimization when considering the prediction errors of the RESs and loads, highlighting the stronger adaptability of stochastic optimization to prediction errors. Moreover, the standard deviation of the objective value for rolling optimization based on the day-ahead stochastic optimization scheme is reduced by 42.79% compared to that of rolling optimization based on the deterministic optimization scheme, indicating smaller revisions to the devices and stronger adaptability to prediction errors.

In future work, extending the modeling approach based on the energy bus to interconnected integrated energy networks would be both interesting and useful. Additionally, employing artificial intelligence methods to address multi-time-scale optimization problems will provide further improvements.

Author Contributions: Conceptualization, L.Z. and F.L.; methodology, L.Z. and F.L.; software, L.Z.; validation, L.Z. and F.L.; data curation, L.Z.; writing—original draft preparation, L.Z.; writing—review and editing, F.L.; visualization, L.Z. and F.L.; supervision, F.L.; project administration, F.L.; funding acquisition, F.L. All authors have read and agreed to the published version of the manuscript.

Funding: This research was funded by the National Natural Science Foundation of China, grant number: 62103239.

Data Availability Statement: The original contributions presented in the study are included in the article; further inquiries can be directed to the corresponding author/s.

Acknowledgments: This research was supported by the National Natural Science Foundation of China (grant number 62103239).

Conflicts of Interest: The authors declare no conflicts of interest.

References

1. Ji, W.; Guo, S.; Sun, H.; Liu, D. Optimal dispatching of multi-community electric-thermal integrated energy systems considering wind and solar uncertainties based on hydraulic stability and energy sharing. *Energy Convers. Manag.* **2024**, *308*, 118335. [[CrossRef](#)]
2. Su, B.; Wang, R.; Wang, M.; Wang, M.; Zhao, Q.; Lv, Y.; Gao, H. Low-Carbon Economic Dispatch of Integrated Energy Systems in Industrial Parks Considering Comprehensive Demand Response and Multi-Hydrogen Supply. *Appl. Sci.* **2024**, *14*, 2381. [[CrossRef](#)]
3. Huang, W.; Zhang, N.; Yang, Y.; Wang, Y.; Kang, C. Optimal configuration planning of multi-energy systems considering distributed renewable energy. *IEEE Trans. Smart Grid* **2019**, *10*, 1452–1464. [[CrossRef](#)]
4. Geidl, M.; Koeppl, G.; Favre-Perrod, P.; Klöckl, B.; Andersson, G.; Fröhlich, K. Energy hubs for the future. *IEEE Power Energy Mag.* **2007**, *5*, 24–30. [[CrossRef](#)]
5. Wang, Y.; Zhang, N.; Kang, C.; Kirschen, D.; Yang, J.; Xia, Q. Standardized matrix modeling of multiple energy systems. *IEEE Trans. Smart Grid* **2019**, *10*, 257–270. [[CrossRef](#)]
6. Liu, T.; Zhang, D.; Dai, H.; Wu, T. Intelligent modeling and optimization for smart energy hub. *IEEE Trans. Ind. Electron.* **2019**, *66*, 9898–9908. [[CrossRef](#)]
7. Wang, Y.; Cheng, J.; Zhang, N.; Kang, C. Automatic and linearized modeling of energy hub and its flexibility analysis. *Appl. Energy* **2018**, *211*, 705–714. [[CrossRef](#)]

8. Ma, S.; Mi, Y.; Shi, S.; Li, H.; Xing, H.; Wang, P. Low-carbon economic operation of energy hub integrated with linearization model and nodal energy-carbon price. *Energy* **2024**, *294*, 130754. [[CrossRef](#)]
9. Li, J.; Yang, S.; Zhou, X.; Li, J. Multi-objective optimization of regional integrated energy system matrix modeling considering exergy analysis and user satisfaction. *Int. J. Elec. Power* **2024**, *156*, 109765. [[CrossRef](#)]
10. Mohammadi, M.; Noorollahi, Y.; Mohammadi-ivatloo, B.; Yousefi, H. Energy hub: From a model to a concept—A review. *Renew. Sustain. Energy Rev.* **2017**, *80*, 1512–1527. [[CrossRef](#)]
11. Mohammadi, M.; Noorollahi, Y.; Mohammadi-ivatloo, B.; Hosseinzadeh, M.; Yousefi, H.; Khorasani, S. Optimal management of energy hubs and smart energy hubs—A review. *Sustain. Energy Rev.* **2018**, *89*, 33–50. [[CrossRef](#)]
12. Bozchalui, M.; Hashmi, S.; Hassen, H.; Cañizares, C.; Bhattacharya, K. Optimal operation of residential energy hubs in smart grids. *IEEE Trans. Smart Grid* **2012**, *89*, 1755–1766. [[CrossRef](#)]
13. Paudyal, S.; Canizares, C.; Bhattacharya, K. Optimal operation of industrial energy hubs in smart grids. *IEEE Trans. Smart Grid* **2015**, *6*, 684–694. [[CrossRef](#)]
14. Vahid-Pakdel, M.; Nojavan, S.; Mohammadi-ivatloo, B.; Zare, K. Stochastic optimization of energy hub operation with consideration of thermal energy market and demand response. *Energy Convers. Manag.* **2017**, *145*, 117–128. [[CrossRef](#)]
15. Rastegar, M.; Fotuhi-Firuzabad, M.; Zareipour, H.; Moeini-Aghaie, M. A probabilistic energy management scheme for renewable-based residential energy hubs. *IEEE Trans. Smart Grid* **2017**, *8*, 2217–2227. [[CrossRef](#)]
16. Brahman, F.; Honarmand, M.; Jadid, S. Optimal electrical and thermal energy management of a residential energy hub, integrating demand response and energy storage system. *Energy Build.* **2015**, *90*, 65–75. [[CrossRef](#)]
17. Ma, T.; Wu, L.; Hao, L.; Li, D. Energy flow matrix modeling and optimal operation analysis of multi energy systems based on graph theory. *Appl. Therm. Eng.* **2019**, *146*, 648–663. [[CrossRef](#)]
18. Luo, X.; Liu, Y.; Liu, J.; Liu, X. Energy scheduling for a three-level integrated energy system based on energy hub models: A hierarchical Stackelberg game approach. *Sustain. Cities Soc.* **2020**, *52*, 101814. [[CrossRef](#)]
19. Dini, A.; Hassankashi, A.; Pirouzi, S.; Lehtonen, M.; Arandian, B.; Baziar, A. A flexible-reliable operation optimization model of the networked energy hubs with distributed generations, energy storage systems and demand response. *Energy* **2022**, *239*, 121923. [[CrossRef](#)]
20. Salehimaleh, M.; Akbarimajd, A.; Dejamkhooy, A. A shrinking-horizon optimization framework for energy hub scheduling in the presence of wind turbine and integrated demand response program. *Sustain. Cities Soc.* **2022**, *79*, 103689. [[CrossRef](#)]
21. Pan, G.; Gu, W.; Wu, Z.; Lu, Y.; Lu, S. Optimal design and operation of multi-energy system with load aggregator considering nodal energy prices. *Appl. Energy* **2019**, *239*, 280–295. [[CrossRef](#)]
22. Chicco, G.; Mancarella, P. Matrix modelling of small-scale trigeneration systems and application to operational optimization. *Energy* **2009**, *34*, 261–273. [[CrossRef](#)]
23. Liu, M.; Shi, Y.; Fang, F. Optimal power flow and PGU capacity of CCHP systems using a matrix modeling approach. *Appl. Energy* **2013**, *102*, 794–802. [[CrossRef](#)]
24. Meng, Q.; Zu, G.; Ge, L.; Li, S.; Xu, L.; Wang, R.; He, K.; Jin, S. Dispatching Strategy for Low-Carbon Flexible Operation of Park-Level Integrated Energy System. *Appl. Sci.* **2022**, *12*, 12309. [[CrossRef](#)]
25. Bao, Z.; Zhou, Q.; Yang, Z.; Yang, Q.; Xu, L.; Wu, T. A multi time-scale and multi energy-type coordinated microgrid scheduling solution—Part I: Model and methodology. *IEEE Trans. Power Syst.* **2015**, *30*, 2257–2266. [[CrossRef](#)]
26. Luo, Z.; Wu, Z.; Li, Z.; Cai, H.; Li, B.; Gu, W. A two-stage optimization and control for CCHP microgrid energy management. *Appl. Therm. Eng.* **2017**, *125*, 513–522. [[CrossRef](#)]
27. Gu, W.; Luo, Z.; Wu, Z.; Li, Z.; Cai, H.; Li, B.; Gu, W. An online optimal dispatch schedule for CCHP microgrids based on model predictive control. *IEEE Trans. Smart Grid* **2017**, *8*, 2332–2342. [[CrossRef](#)]
28. Li, X.; Wang, W.; Wang, H. Hybrid time-scale energy optimal scheduling strategy for integrated energy system with bilateral interaction with supply and demand. *Appl. Energy* **2021**, *285*, 116458. [[CrossRef](#)]
29. Hu, K.; Wang, B.; Cao, S.; Li, W.; Wang, L. A novel model predictive control strategy for multi-time scale optimal scheduling of integrated energy system. *Energy Rep.* **2022**, *8*, 7420–7433. [[CrossRef](#)]
30. Song, Y.; Mu, H.; Li, N.; Wang, H.; Kang, X. Optimal scheduling of zero-carbon integrated energy system considering long- and short-term energy storages, demand response, and uncertainty. *J. Clean. Prod.* **2024**, *435*, 140393. [[CrossRef](#)]
31. Li, X.; Wang, H. Integrated energy system model with multi-time scale optimal dispatch method based on a demand response mechanism. *J. Clean. Prod.* **2024**, *445*, 141321. [[CrossRef](#)]
32. Wang, G.; Pan, C.; Wu, W.; Fang, J.; Hou, X.; Liu, W. Multi-time scale optimization study of integrated energy system considering dynamic energy hub and dual demand response. *Sustain. Energy Grids* **2024**, *38*, 101286. [[CrossRef](#)]
33. Wang, J.; Sui, J.; Jin, H. An improved operation strategy of combined cooling heating and power system following electrical load. *Energy* **2015**, *85*, 654–666. [[CrossRef](#)]
34. Zhang, Y.; Liu, Z.; Wu, Y.; Li, L. Research on Optimal Operation of Regional Integrated Energy Systems in View of Demand Response and Improved Carbon Trading. *Appl. Sci.* **2023**, *13*, 6561. [[CrossRef](#)]
35. Xu, Y.; Zhang, S.; Xiao, Y. Modeling the dynamic simulation and control of a single effect LiBr–H₂O absorption chiller. *Appl. Therm. Eng.* **2016**, *107*, 1183–1191. [[CrossRef](#)]

36. Huang, Y.; Wang, W.; Hou, B. A hybrid algorithm for mixed integer nonlinear programming in residential energy management. *J. Clean. Prod.* **2019**, *226*, 940–948. [[CrossRef](#)]
37. Zhu, L.; Wang, G.; Li, Y.; Duo, Z.; Sun, C. Optimization of hydrogen liquefaction process based on parallel genetic algorithm. *Int. J. Hydrogen Energy* **2022**, *47*, 27038–27048. [[CrossRef](#)]

Disclaimer/Publisher’s Note: The statements, opinions and data contained in all publications are solely those of the individual author(s) and contributor(s) and not of MDPI and/or the editor(s). MDPI and/or the editor(s) disclaim responsibility for any injury to people or property resulting from any ideas, methods, instructions or products referred to in the content.